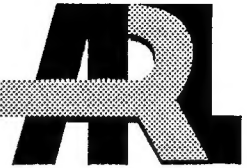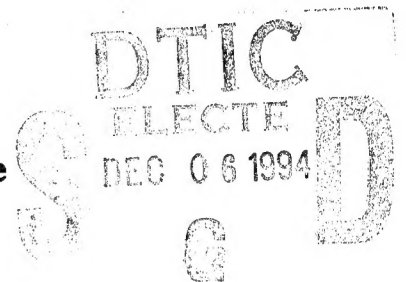ARMY RESEARCH LABORATORY

Indexing Meso-β Surface Wind Site Representative

Martin E. Lee
Teizi Henmi
Battlefield Environment Directorate

DTIC
ELECTE
DEC 06 1994
D

ARL-TR-284   September 1994

19941129 101

Approved for public release; distribution is unlimited.

NOTICES

Disclaimers

The findings in this report are not to be construed as an official Department of the Army position, unless so designated by other authorized documents.

The citation of trade names and names of manufacturers in this report is not to be construed as official Government indorse-ment or approval of commercial products or services referenced herein.

Destruction Notice

When this document is no longer needed, destroy it by any method that will prevent disclosure of its contents or reconstruction of the document.

REPORT DOCUMENTATION PAGE

Public reporting burden for this collection of information is estimated to average 1 hour per response, including the time for reviewing instructions, searching existing data sources, gathering and maintaining the data needed, and completing and reviewing the collection of information. Send comments regarding this burden estimate or any other aspect of this collection of information, including suggestions for reducing this burden, to Washington Headquarters Services, Directorate for Information Operations and Reports, 1215 Jefferson Davis Highway, Suite 1204, Arlington, VA 22202-4302, and to the Office of Management and Budget, Paperwork Reduction Project (0704-0188), Washington, DC 20503.

1. AGENCY USE ONLY *(Leave blank)*	2. REPORT DATE September 1994	3. REPORT TYPE AND DATES COVERED Final

4. TITLE AND SUBTITLE

Indexing Meso-β Surface Wind Site Representative

5. FUNDING NUMBERS

6. AUTHOR(S)

Martin E. Lee and Teizi Henmi

7. PERFORMING ORGANIZATION NAME(S) AND ADDRESS(ES)

U.S. Army Research Laboratory
Battlefiled Environment Directorate
ATTN: AMSRL-BE-W
White Sands Missile Range, NM 88002-5501

8. PERFORMING ORGANIZATION REPORT NUMBER

ARL-TR-284

9. SPONSORING / MONITORING AGENCY NAME(S) AND ADDRESS(ES)

U.S. Army Research Laboratory
2800 Powder Mill Road
Adelphi, MD 20783-1145

10. SPONSORING / MONITORING AGENCY REPORT NUMBER

11. SUPPLEMENTARY NOTES

12a. DISTRIBUTION / AVAILABILITY STATEMENT

Approved for public release; distribution is unlimited

12b. DISTRIBUTION CODE

13. ABSTRACT *(Maximum 200 words)*

Multiple meso-β surface wind site data representativeness is examined in a comparison of corresponding sets of surface mesoscale model windfield predictions - with and without periodic surface data assimilation. A version of the Higher Order Turbulence Model for Atmospheric Circulation (HOTMAC) is used in this study to obtain selected surface gridded windfields. Six different radiosonde initialization data sets are used to generate seven hour HOTMAC surface windfield predictions. Two series of HOTMAC simulations are executed: a control case with sparse radiosonde initialization data (≤ 6 observations); and an experimental case, in which supplementary hourly surface wind observations, obtained from a consistent set of fifteen automated surface observation stations over a meso-β scale complex terrain area, are also periodically assimilated into HOTMAC windfields by locally adjusting predicted windfield solutions toward observed conditions and correcting for mass conservation imbalances in the adjusted fields. After observation site data are interpolated from both gridded HOTMAC control and experimental surface windfield predictions, factor separation and statistical tests are used to characterize the representativeness of available surface observation stations in the modeled meso-β scale regime. Conclusions and the implications of presented results are summarized.

14. SUBJECT TERMS

Higher order turbulence model for atmospheric circulation, numerical weather protection, target area meteorological data experiment

15. NUMBER OF PAGES

41

16. PRICE CODE

17. SECURITY CLASSIFICATION OF REPORT Unclassified	18. SECURITY CLASSIFICATION OF THIS PAGE Unclassified	19. SECURITY CLASSIFICATION OF ABSTRACT Unclassified	20. LIMITATION OF ABSTRACT SAR

Preface

The purpose of this report is to describe a structured method that can be used to identify the potential magnitude/s and significance of meteorological scale-decoupling between specific surface wind observation sites and a meso-β scale prognostic model. This work is related to studies that have examined the climatologically optimal placement of surface sensors over complex terrain. However, results in this study are derived using a meso-β scale model in conjunction with a diverse set of diurnally varying, nearly meso-γ scale surface wind observation data, not mean climatological data.

Accesion For		
NTIS CRA&I		☒
DTIC TAB		☐
Unannounced		☐
Justification		
By		
Distribution /		
Availability Codes		
Dist	Avail and / or Special	
A-1		

1

Contents

Figures

Tables

Executive Summary

Introduction

Multiple meso-β * surface wind site data representativeness is examined here in a comparison of corresponding sets of surface mesoscale model windfield predictions, with (experimental case) and without (control case) periodic surface data assimilation.

Purpose

This investigation was conducted to identify the potential magnitude/s and significance of scale-decoupling between specific observation sites and meso-β scale model prognostic assumptions.

Overview

A version of the *Higher Order Turbulence Model for Atmospheric Circulation* (HOTMAC), which has been applied to a large variety of meso-β scale research and applications, is used in this study to obtain selected surface gridded windfields. Six different radiosonde initialization data sets are used to generate HOTMAC seven hour surface windfield predictions using: 1) a control case with sparse radiosonde initialization data ($\leq$ six observations); and 2) an experimental case, in which supplementary hourly surface wind observations, obtained from a consistent set of 15 non-uniformly distributed, automated surface observation stations over a meso-β scale complex terrain area, are also periodically assimilated into HOTMAC windfields by locally adjusting predicted windfield solutions toward observed conditions and correcting for mass conservation imbalances in the adjusted fields. Factor separation and statistical tests are used to characterize the degree of surface observation station scale-coupling to the modeled meso-β scale wind field forecasts.

Conclusions

The *mean index* developed for use in this study, weighted against testing *significance levels*, is an effective means with which extremely unrepresentative, unpredictable site data can be objectively ranked, and then selectively filtered out to improve the dynamical consistancy of initialization data sets.

Spatial scale ranges are approximately 2 km $\leq$ Meso-β scale $\leq$ 200 km.

Recommendations

The diverse range of individual surface observation site ensemble comparison results found in this study demonstrate that surface data sets require careful analysis to identify each site's scale-suitability prior to inclusion in a meso-β scale model initialization scheme.

1. Introduction

Determining optimal, dynamically consistent initial conditions for making predictions is the goal of a good Numerical Weather Prediction (NWP) initialization scheme. However, many errors can be introduced into initial condition data. For example, data void regions yield insufficient data density to resolve mesoscale features, and the behavior of features that are not measured will probably not be predicted very well. Other possible sources of initial condition errors include observation errors resulting from instrument performance problems as well as coding and transmission mistakes. The representativeness of observation data is another possible source of initialization condition errors.[1] It is the representativeness problem of meso-β scale [2] initial condition and periodic assimilation surface wind data that is investigated in this study.

This study centers on the problem of meso-β surface wind data representativeness. Comparison and analysis is made of simulated meso-β scale anabatic and katabataic, thermally direct, diurnally induced and gravity forced circulations over complex terrain with and without supplemental surface data assimilation.[3] Meso-β scale anabatic and katabataic circulations that interact with a slowly varying ensemble flow, with otherwise weak synoptic forcing (i.e., the main scale interaction † in this study is essentially limited to the influence of mean flow on localized, meso-β circulations).

The importance of mesoscale interactions was recogonized by the U.S. Army as early as 1951 from the radar research results of Ligda [2]; the term *mesoscale* was actually first introduced by Ligda in a U.S. Army sponsored work.[4] The U.S. Army today has a continued, increasing interest in understanding more about mesoscale interactions, that can have a significant influence on battlefield operations. For example, wind variability within the sphere of influence of the mesoscale can significantly influence artillery accuracy.

Accurate short-range windfield forecasts are also becoming crucial to other U.S. Army field operations, such as in predicting atmospheric effects on chemical fallout.[6] As a result, a need exists for the U.S. Army to decrease meteorological uncertainty and errors in wind field

---

†*Identification of scale differentiation and interactions originated primarily from comparing observations of atmospheric phenomena to varying observation network resolutions; this was followed by making theoretical inferences [4], a process that could be carried out using factor separation.[5]*

predictions. Solutions to this problem translate into various unit performance improvements: for example, the effectiveness of artillery fire.[7] Characterizing the representativeness of mesoscale observation data is an important issue (e.g., in the development of mesoscale windfield prediction decision aids for the U.S. Army). This study examines the representativeness problem using a limited set of surface wind observation data that is selectively incorporated as initial condition and periodic assimilation data into a mesoscale atmospheric circulation model.

2. Numerical modeling methods

2.1 Description of the model

A version of the *Higher Order Turbulence Model for Atmospheric Circulation* (HOTMAC), a second-moment turbulence-closure model, is used in this study to obtain selected 4d surface windfield gridded outputs. The HOTMAC model is very effective in predicting meso-β scale drainage and upslope surface winds [8][9], especially under relatively weak synoptic forcing; under these conditions, external differential surface heating effects, which are estimated by HOTMAC, and gravitational forcing over complex terrain play critical roles.[3]

HOTMAC computes geostrophic wind components using the hydrostatic assumption and applies a Boussinesq approximation incorporating a terrain following vertical coordinate system:

$$z^* = \overline{H}\frac{z - z_g}{H - z_g},\tag{1}$$

where z^* and z are the transformed and Cartesian vertical coordinates, respectively; z_g represents terrain elevation above sea level (ASL); $\overline{H}$ is the material surface upper boundary of the model in z^* coordinates and H is the corresponding z coordinate height.

The governing conservation-of-momentum equation in the x direction, following the coordinate transformation, is

$$
\begin{aligned}
\frac{DU}{Dt} &= f(V - V_g) + g\frac{\overline{H} - z^*}{\overline{H}}\left(1 - \frac{<\theta_v>}{\theta_v}\right)\frac{\partial z_g}{\partial x} \\
&+ \frac{\partial}{\partial x}\left(K_x\frac{\partial U}{\partial x}\right) + \frac{\partial}{\partial y}\left(K_{xy}\frac{\partial U}{\partial y}\right) + \frac{\overline{H}}{H - z_g}\left[\frac{\partial}{\partial z^*}(-\overline{uw})\right] \\
&- \eta\, C_d\,[\,a(z)\,U\cdot S\,] + G(U_t - U),
\end{aligned}\tag{2}
$$

where $< \ >$ indicates an average over a horizontal surface, f is the Coriolis parameter, g is acceleration due to gravity, θ_v represents virtual potential temperature fluctuations, and K_x and K_{xy} are horizontal eddy viscosity coefficients; C_d is a canopy drag coefficient, $a(z)$ is the plant area density, η is the fraction $(0 \leq \eta \leq 1)$ of area covered by trees, and $S = \sqrt{U^2 + V^2 + W^2}$. The pressure gradient force term is expressed in terms of: 1) V_g, or the geostrophic V component; and 2) the second term on the right-hand side of equation (2). Mean turbulent momentum flux is represented as $\overline{uw}$, the next to the last term on the right-hand side of equation (2) represents drag force due to tree canopies, and the last term nudges the horizontal modeled wind fields, U, to target winds, U_t.[10] ‡

2.2 Case-specific model characteristics

A version of HOTMAC was configured to make hourly forecasts out to 7 h from two initialization times (0600L and 1400L); there were 18×22 modeled horizontal grid points and 31 model layers AGL with an upper boundary ≈ 15 km ASL. The southwest terrain anchor was located at lat. 32.984 N, long. 106.241 W, with 8.0 km model grid resolution both in the x and y directions. Minimum terrain elevation was 1,185.0 m ASL, and maximum terrain elevation was 3,075 m ASL. Only available radiosonde data were used to initialize HOTMAC (see table 1). Only the $\overline{z} \approx 10 \ m$ AGL surface windfield outputs were used in this study and the nudging factor G was held constant at $G \equiv 5.0 \times 10^{-4}$.

2.3 Data assimilation modification to the model

A modified objective analysis procedure was used to convolve gridded HOTMAC predictions of surface windfields with corresponding, consistent sets of randomly spaced surface wind observations. This procedure was used to periodically constrain HOTMAC windfield predictions to surface wind observation data as it became available. The goal was to adjust HOTMAC windfield predictions (and analyses at

---

‡ *Target winds, as defined in [10], are obtained by solving the equations of motion; for example, in the x direction, incorporating observed and geostrophic components as in*

$$U_t = U_{obs} - \frac{f}{C_n}(V_{obs} - V_g), \tag{3}$$

without frictional effects, where C_n is a constant nudging coefficient. Thus, the nudging term adjusts winds toward observation data in the free atmosphere but has little effect in the boundary layer where frictional effects become significant. Also, $C_n = G$, and both C_n and G operate in equation (2).

t_o) as closely as possible to available surface wind observations without eliminating the windfield dynamics predicted by HOTMAC in data sparse regions. This procedure was used to perform periodic reanalyses of hourly HOTMAC windfield outputs.

The modified objective analyses took an initial HOTMAC gridded surface windfield ξ and a randomly spaced set of n surface wind observations.[11] The mean field error was then calculated and removed from all ξ grid points to produce a field ξ^*. At this point, all ξ^* grid points within $\leq$ one grid square were adjusted to create an adjusted ξ^{**} field defined as follows:

$$\xi^{**} = \xi^* + \frac{\sum_{i=1}^n d_{mi}^*}{\sum_{i=1}^n W_{mi}}, \tag{4}$$

where d_i^* is the local discrepancy between observation i and the interpolated ξ^* field at the four surrounding local grid points ($m = 1, 2, 3, 4$); W_{mi} is the local m'th objective weighting factor. Only grid points in the vicinity of the randomly spaced surface wind observations are affected by the ξ^{**} operation. The unaffected ξ^* grid points are then adjusted using iterative relaxation to alleviate edge discontinuity between ξ^* and ξ^{**} gridded fields; this results in a ξ^{***} gridded field that has the following property

$$\nabla^2 \xi^{***} \simeq \nabla^2 \xi^*, \tag{5}$$

The purpose of this objective analyses was to use the largest set of consistently reported surface wind observations in selectively adjusting HOTMAC windfield predictions to corresponding observation data.

Reanalyzed HOTMAC surface windfields were then further adjusted for mass consistency by iteratively reducing divergence, where divergence is defined as follows:

$$\frac{\partial u}{\partial x} + \frac{\partial v}{\partial y} = \phi(i, j), \tag{6}$$

where u is the west-east wind component, v is the south-north wind component, and $\phi(i, j)$ is the divergence at each grid point.[12] The combination of the modified objective analysis and mass consistency operations represent the data assimilation scheme employed in this study. Advantages of this basic assimilation scheme are primarily its economy of computational resources, processing time, and input data requirements.

10

3. Meteorological Scenarios

Meteorological observation data, consisting of radiosonde and automated surface wind observations ($\simeq 10\,m$ AGL), were obtained for three separate days (Julian days 167, 246, and 272 in 1992) in a $136 \times 168\ \text{km}^2$ area centered over a complex terrain region (elevation extremes: 1,185.0 m - 3,075.0 m ASL; absolute terrain differential = 1,890 m) in southern New Mexico (see figure 1). This data was acquired during portions of a Target Area Meteorological Data Experiment (TAMDE) conducted by the U.S. Army Research Laboratory (ARL), Battlefield Environment Directorate (BED). TAMDE was implemented to study the variability of weather and weather effects on a variety of weapon and fire control systems.[6]

TAMDE radiosonde data used to initialize the control and experimental HOTMAC simulations are identified in table 1. Three sets of hourly surface wind observation data, corresponding to Julian days 167, 246, and 272 in 1992, were collected for the experimental assimilation portion of this study. The 10 m AGL surface wind observations were obtained from a consistent network of 15 automated surface observation sites (relative sensor locations indicated in figure 1) that were configured to log 15 minute averaged observation data.

4. Experiment Design

4.1 Control case

In the control case, hourly surface wind data were objectively analyzed using the following basic interpolation scheme:

$$U(i,j) = \sum_{m=1}^{n} \psi_m(r)U_m / \sum_{m=1}^{n} \psi_m(r), \qquad (7)$$

where $U(i,j)$ is the calculated value at the grid point (i,j), U_m is the observed wind at site m, $\psi_m(r) \equiv \frac{1}{r^2}$, and r is the grid point to observation site distance. Following the $1/r^2$ interpolation of observed surface winds to gridded fields, the gridded fields were adjusted for mass consistency using iteratively reduced divergence to a predefined threshold, where divergence is defined as follows:

$$\frac{\partial u}{\partial x} + \frac{\partial v}{\partial y} = \phi(i,j), \qquad (8)$$

where u is the west-east wind component, v is the south-north wind component, and $\phi(i,j)$ is the divergence at each grid point.[12]

4.2 Experimental case

In the *experimental* case a modified objective analysis procedure, summarized in equations (4- 6), was used to convolve gridded HOTMAC surface windfield predictions with corresponding sets of irregularly spaced surface wind observations; this periodically constrained HOTMAC windfield predictions to surface wind observation data. Therefore, resulting surface windfield predictions were a function of both: 1) HOTMAC meso-β prognostic atmospheric dynamics considerations; and 2) the selected surface observation data.

4.3 Data analysis techniques

Because anabatic (katabatic) circulation interactions over a complex terrain domain often produce confluent (diffluent) flow in valleys (along ridgelines), comparing individual points in HOTMAC surface windfield predictions to mean windfield statistical properties is of little assistance in characterizing the true meso-β scale represesentativeness of a particular observation site. Instead, the corresponding *control* and *experimental* case results need to be compared at each point that contributed observation data to this study.

Factor separation was used to compute interactions of the *experimental* case factor influencing HOTMAC surface windfield predictions.[5] The interaction factor investigated in this study is meso-β scale surface wind unpredictability, λ, which is inversely related to observation site representativeness; λ is the effect of periodically assimilated surface data on a meso-β scale HOTMAC *base case* simulation field, $f(0)$. Factor λ is multiplied by a changing coefficient c, where $0 \le c \le 1$ in the following:

$$\lambda(c) = c\lambda, \qquad (9)$$

which produces a resulting field f that is a continuous function of c:

$$f = f(c), \qquad (10)$$

where function $f(c)$ can be decomposed into: 1) a constant part that is independent of c, $\hat{f}_o$, which is a short form of $\hat{f}(0)$ and represents the fraction of f that does not depend on factor λ; and 2) a c dependent component, $\hat{f}(c)$.

In this case, the surface windfield unpredictability, $\hat{f}(c)$, can be expressed as follows:

$$\hat{f}(c) = f(c) - f_o, \qquad (11)$$

where $f(c)$ is the value of a predicted *experimental case* HOTMAC surface windfield that is a continuous function of c, and f_o is the value of f in the control simulation that has factor λ omitted.

Table 1. TAMDE radiosonde data used to initialize HOTMAC *control* and *experimental* simulations. (availability indicated with a ● symbol).

DATE	TIME	UA Station No.					
		1	2	3	4	5	6
167	0600		●				
	1400		●				
246	0600			●	●		●
	1400	●	●	●	●	●	
272	0600	●	●	●		●	
	1400	●	●	●	●	●	●

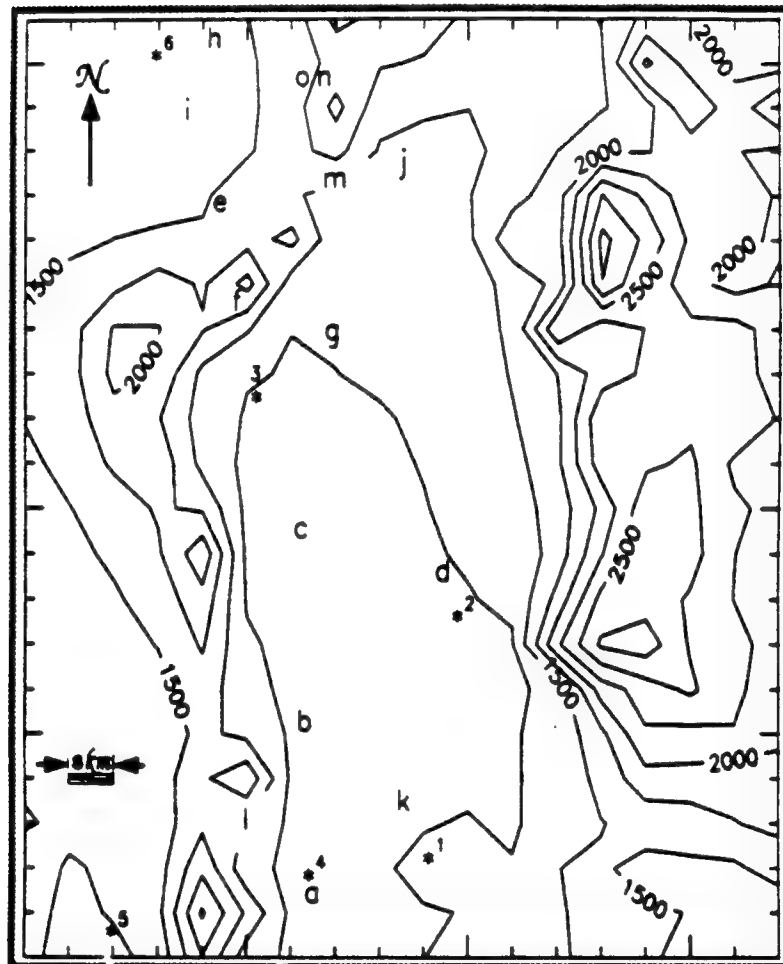Figure 1. Model surface terrain elevation ASL (contour interval = 250 m, area = 136 km × 168 km). Automated surface (radiosonde) observation site locations are indicated by corresponding site alpha (∗ numeric) symbols.

In this study, $\hat{f}(c)$ is statistically analyzed to isolate and resolve the inversely related representativeness of selected observation site data to the simulated HOTMAC meso-β scale regime of anabatic/katabatic boundary layer circulation interactions using the following measures of the $\hat{f}(c)$ surface u and v wind component: 1) correlation and scatter; 2) relative mean bias; 3) percentage of cases within a factor of two; 4) mean and upper/lower bound differences; 5) *F-test* for significance of variance differences; 6) *Student's t-test* for significance of differences in means; 7) *Kolmogorov-Smirnov test* for significance in cumulative distribution function differences; and 8) *Chi-Square test* for significance in population distribution differences.[13][14][15]

5. Results

The $\hat{f}(c) = \sqrt{[\hat{f}(c)_u]^2 + [\hat{f}(c)_v]^2}$ combined results for each surface observation site (see figure 1) are illustrated in figure 2, where $R \equiv \hat{f}(c)$, and the following is true:

$$\hat{f}(c)_u = u_{experimental} - u_{control}, \tag{12}$$

$$\hat{f}(c)_v = v_{experimental} - v_{control}. \tag{13}$$

Results from this test indicate that sites 1, 4, and 11 had the smallest $\hat{f}(c)$ differences ($\leq$ 2.4 m/s) and are, therefore, the most representative meso-β scale sites. Conversely, sites 8, 10, and 13 had the largest $\hat{f}(c)$ differences ($\geq$ 3.0 m/s), and, according to this test result, were the least representative meso-β scale sites.

The R comparisons in figure 2 were integrated into the measure of $\hat{f}(c)$ mean and upper/lower bound differences (test number 4, from section **4.c**). The remaining seven $\hat{f}(c)_u$ and $\hat{f}(c)_v$ tests mentioned in section **4.c** were applied to $\hat{f}(c)$ data interpolated at each surface observation site (figure 1) from *control* and *experimental* simulation results. All significant test results are summarized in table 2, where a "•" ("⊗") symbol indicates high confidence in identifying relatively small (large) values of $\hat{f}(c)$; small, relative $\hat{f}(c)$ results for particular tests, at particular sites, indicate a higher degree of meso-β scale representativeness.

A simple *mean index* scheme was devised to summarize the net test results for each observation site (see table 2). The *mean index* for each site was calculated by dividing the number of representative test results ("•" symbols from table 2) by the sum of all high confidence test result relative rankings ("•" and "⊗" symbols from table 2). Therefore, higher (lower) *mean index* values are associated with relatively more representative (unrepresentative) sites. For example,

sites 14 and 15 have perfect *mean index* values (1.0) and, without considering any other factors, are the most representative observation sites. Conversely, sites 3 and 12 had *mean index* values ≤ 0.17, indicating the lowest degree of relative meso-β scale observation site agreement.

However, *mean index* values are also a function of the total number of high confidence test results per observation site. Thus, the *mean index* values require further interpretation. For example, the *mean index* can be weighted against its *significance level*. For the purposes of this study, a *mean index - significance level* was defined as the cumulative number of high confidence test results divided by the total number of tests used ($n = 8$). Table 2 lists *significance levels* and *mean index* values for each site, and figure 3 presents a graphical comparison of both *significance level* and the *mean index* for each site. Figure 3 indicates that site 3 scored the highest *significance level* (1.0), while sites 5, 14, and 15 had the lowest *significance levels* (0.25).

6. Summary and Conclusions

This study was implemented to investigate the representativeness of operationally available data. The goal was to identify how well available observations from a given set of observation sites compared to reliably predicted meso-β scale circulation features. The *mean index* derived in this study (see table 2) is a simple approach to the complex quality control problem of classifying relative representativeness of meso-β scale observation sites in a complex terrain setting. The *mean index*, defined in section 5, can be used to characterize the spectrum of individual observation site agreement with dynamicaly balanced katabatic/anabatic meso-β scale modeled circulation interaction in complex terrain settings; this provides objective guidance on a particular observation site's meso-β scale representativeness.

The $\hat{f}(c)$ results in figure 2 agreed very well with the *mean index* results (see table 2). For example, sites 1, 4, and 11 had the lowest R values (figure 2) and all three of these sites scored significantly above the average *mean index* results (.83, .75, and .75, respectively, with ≥ 4 independent test indicators, or having *significance levels* $\geq .50$); these combined results characterize sites 1, 4, and 11 as the most representative at the meso-β scale. Conversely, sites 3, 8, and 13 had below average *mean index* results (.13, .33, and .43, respectively, with ≥ 6 independent test indicators, or having *significance levels* $\geq .75$), and all three of these sites had the highest R values (figure 2).

For site 10, $R > 3.0$ m/s, which was greater than R results for sites 3 and 12 (see figure 2). However, only three out of eight possible independent test indicators in table 2 could clearly differentiate site 10 relative representativeness (*significance level* of .38). Therefore, site 10 results were not considered in further relative site rankings. Site 12 did not have a greater R value than sites 3, 8, or 13 (figure 2); in contrast to site 10 inferences, site 12 scored the second lowest *mean index* (.17 – determined by 6 test indicators, a *signifcance level* of .75), and was classified as an unrepresentative observation site. Thus, the least representative observation sites in this study include sites 3, 8, 12, and 13. These results illustrate: 1) why site representativeness conclusions should not be dependent on only one test result; 2) how the cumulative comparisons of the number of test indicators can become a significant analysis/decision factor.

From figure 1, sites 12 (**l**) and 13 (**m**) are located along the eastern slopes of mountainous ridgelines with terrain elevations varying ≥ 500 m within a 1 km radius of each of these sites. Unpredictable mechanical turbulence effects, forced by the significant variations in local terrain elevation, are probable causes for the relatively unrepresentative ranking of these two sites. Similarly, site 3 (**c**) is within ≈ 2 km of steep terrain rise (≥ 750 m) to the west. Site 8 (**h**) is a difficult observation site in this study because of its vicinity to the northern model boundary condition (< 1 km within the model domain); in this case, the observation site may be more accurate at the meso-β scale than simulation results approaching model domain limits.

Conversely, sites 4 (**d**) and 11 (**k**) are nested ≥ 3 km within the model domain, and are located on relatively smooth local terrain with minimal relative slope changes; this is probably why these two sites ranked as highly as representative at the meso-β scale in terms of their corresponding R, *mean index*, and *significance level* Similar to site 3 (**c**), site 1 (**a**) is within ≈ 2 km of a steep change in terrain (≥ 1 km), yet like sites 4 (**d**) and 11 (**k**), it is located on relatively smooth local terrain, and also ranked as highly representative at the meso-β scale; Site 1 (**a**) thus illustrates why spatial terrain analysis alone provides insufficient guidance on the meso-β scale boundary layer representativeness of particular observation sites when other analysis tools, like a valid meso-β scale atmospheric circulation model, are available.

Table 2. Site/test summary matrix, identifying the most representative (least representative) meso-β scale observation sites with a "●" ("⊗") symbol, where test numbers correspond to significant u and/or v surface wind component $\hat{f}(c)$ measures.¶ The *significance level* and *mean index* are defined in section 5.

	SITE		Test No.¶ 1	2	3	4	5	6	7	8	SIGNIFICANCE LEVEL	MEAN INDEX
1	↔	a	●	⊗	●	●	●		●		.75	.83
2	↔	b			●	⊗		⊗	⊗	●	.63	.40
3	↔	c	⊗	⊗	⊗	⊗	●	⊗	⊗	⊗	1.0	.13
4	↔	d			●	●	●			⊗	.50	.75
5	↔	e		●						⊗	.25	.50
6	↔	f		●		⊗		⊗	●		.50	.50
7	↔	g		●			⊗	●			.38	.67
8	↔	h	●		⊗	⊗	⊗		●	⊗	.75	.33
9	↔	i	●					●	●	⊗	.50	.75
10	↔	j	⊗			⊗			⊗		.38	.00
11	↔	k	●		●	●			⊗		.50	.75
12	↔	l	⊗	⊗		⊗		⊗	●	⊗	.75	.17
13	↔	m		●	⊗	⊗	⊗	●	⊗	●	.88	.43
14	↔	n	●					●			.25	1.00
15	↔	o	●					●			.25	1.00
∑ USAGE			9	7	7	10	6	9	10	8	AVG=0.55	AVG=0.54

¶ NOTE: Test Numbers correspond to the following statistical methods:

1 – correlation and scatter;

2 – relative mean bias;

3 – percentage of cases within a factor of two;

4 – mean and upper/lower bound differences;

5 – *F-test* for significance of variance differences;

6 – *Student's t-test* for significance of differences in means;

7 – *Kolmogorov-Smirnov test* for significance in cumulative distribution function differences;

8 – *Chi-Square test* for significance in population distribution differences.
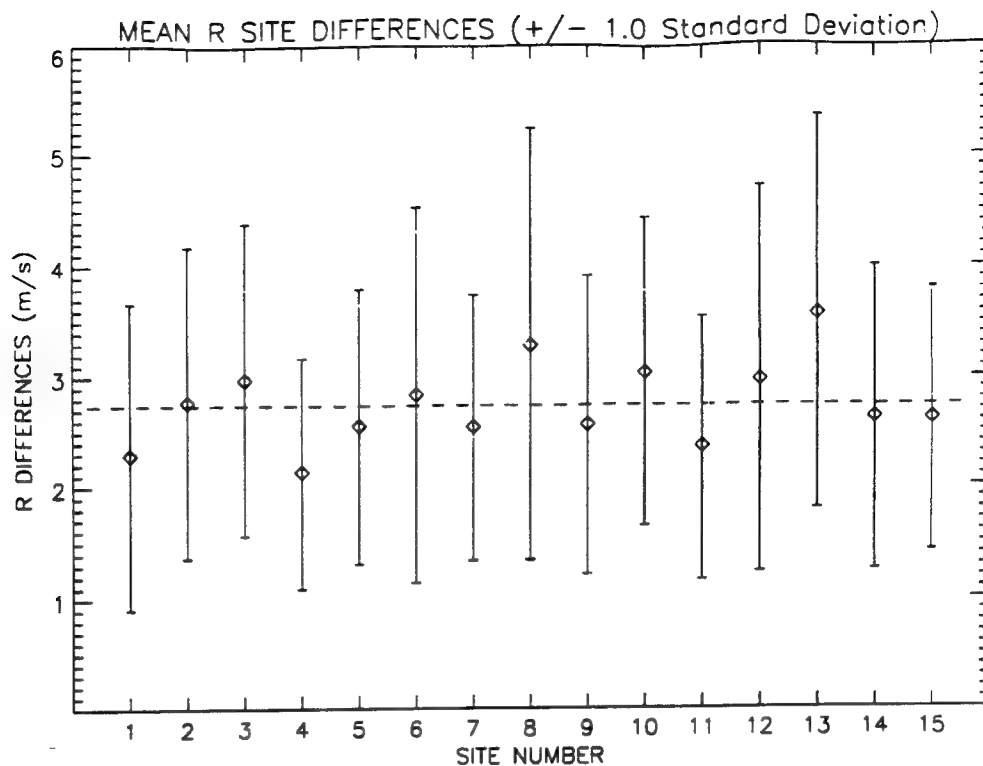
Figure 2. Mean R values, defined in section 5, with ± 1.0 standard deviation tick marks, for each surface wind observation site. Mean R for all sites is also included (horizontal dashed line).
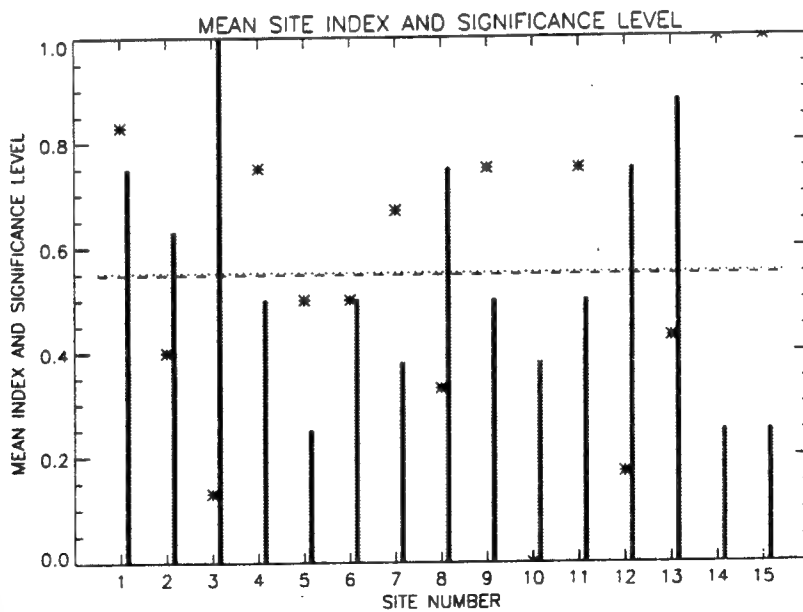
Figure 3. *Mean index* ($*$) and *significance level* (bar chart plot) for each site, with the net average value of each (plotted respectively as a dashed and dotted horizontal line).

The diverse range of individual surface observation site ensemble comparison results in this study demonstrate that surface data sets require careful analysis to identify each site's representativeness prior to inclusion in a meso-β scale model initialization scheme. The *mean index* developed for use in this study, weighted against testing *significance levels*, is an effective means with which extremely unrepresentative, unpredictable site data can be objectively ranked; physically unreasonable site data can then be selectively filtered out to improve the dynamical consistancy of initialization data sets, which will decrease prediction errors when a meso-β scale model is integrated forward in time.[1][16]

Recommendations

Critical field application/s of meso-β scale model forecasts should be accompanied by some type of initialization data quality control that addresses the scale-coupling of observation data to the model assumptions; otherwise, forecast errors may result that are not due to the model. Further classification of observation site data should also include the application of more sophisticated complex quality control schemes that more specifically address other factors such as instrument errror and/or calibration problems; these will be implemented in the planned continuation of this research work.[§]

[§] *Brock [14] suggests some methodology to identify suspect observation data in a preliminary quality assurance audit prior to its incorporation into a model initialization scheme: 1) detailed observation variability intercomparisons; 2) data range testing against preset parameter limits; and 3) applying an impulse noise threshold detection filter to the data.*

References

1. Carr, F., "Introduction to Numerical Weather Prediction and Present/Future Modeling Activities at NMC," *Lecture Notes (November 2, 1993)*, COMET Mesoscale Forecasting and Analysis Course, NCAR, Boulder, CO 80307, 70 pp., 1993.

2. Fujita, T.T., "Mesoscale Classifications: Their History and Their Application to Forecasting," *Mesoscale Meteorology and Forecasting*, Ray, P.S., Ed., *Amer. Meteor. Soc.*, 18 pp., 1986.

3. Huschke, R., Ed., "Glossary of Meteorology." *Amer. Meteor. Soc.*, 638 pp., 1959.

4. Emanuel, K.A., "Overview and Definition of Mesoscale Meteorology," *Mesoscale Meteorology and Forecasting*, Ray, P.S., Ed., *Amer. Meteor. Soc.*, 17 pp., 1986.

5. Stien, U., and Alpert, P., "Factor Separation in Numerical Simulations," *J. Atmos. Sci.*, **50**, 9 pp., 1993.

6. Grace, J., "TAMDE - The Variability of Weather over an Army Division Size Area," 1993 Battlefield Atmospherics Conference Proceedings (under final revision), Battlefield Environment Directorate, White Sands Missile Range, NM 88002, 13 pp., 1993.

7. Blanco, A., and Cogan, J., "Mobile Profiler System Improvements to the MET Error Contribution of the Artillery Error Budget," Battlefield Atmospherics Conference Proceedings, Battlefield Environment Directorate, White Sands Missile Range, NM 88002, 15 pp., 1993.

8. Yamada, T., "A Numerical Model Study of Turbulent Airflow in and Above a Forest Canopy," *J. Meteor. Soc. of Japan*, **60**, 15 pp., 1982.

9. Yamada, T., and Bunker, S., "A Numerical Model Study of Nocturnal Drainage Flows with Strong Wind and Temperature Gradients," *J. Appl. Meteor.*, **28**, 9 pp., 1989.

10. Henmi, T., Dumais, R., and Smith, T, "Operational Short-Range Forecast Model for Battlescale Areas," Battlefield Atmospherics Conference Proceedings, Battlefield Environment Directorate, White Sands Missile Range, NM 88002, 10 pp., 1993.

11. Danard, M., Lyv, G., and MacGillivray, G., "A Mesoscale Bulk Model of the Atmospheric Boundary Layer, Part I, Phases I and II," Technical Report ASL-CR-85-0126-1, Contract No. DAAD07-83-C-0126, U.S. Army Atmospheric Sciences Laboratory, White Sands Missile Range, NM 88002, 61 pp., 1985.

12. Lee, M., "Complex Terrain Wind Model Evaluation," *Thesis*, New Mexico State University, Las Cruces, NM 88003, 149 pp., 1992.

13. Hanna, S., "Mesoscale Meteorological Model Evaluation Techniques, with Emphisis on Needs of Air Quality Models," *contained in AMS Monograph (under final revision) on the 1992 Mesoscale Workshop, El Paso, TX*, 19 pp., 1992.

14. Brock, F. V., "Analysis of the Surface Atmospheric Measurement System, Scientific Services Program Report," Contract No. DAAL03-86-D-001, U.S. Army Atmospheric Sciences Laboratory, White Sands Missile Range, NM 88002, 50 pp., 1990.

15. Press, W., Flannery, B., Teukolsky, S., and Vetterling, W., "Numerical Recipes in C," Cambridge University Press, 735 pp., 1988.

16. Toth, Z., and Kalnay, E., "Ensemble Forecasting at NMC: The Generation of Perturbations," *Bull. Amer. Meteor. Soc.*, **74**, 14 pp., 1993.

Acronyms and Abreviations

AGL	Above Ground Level
ARL	Army Research Laboratory
ASL	Above Sea Level
BED	Battlefield Environment Directorate
HOTMAC	Higher Order Turbulence Model for Atmospheric Circulation
NWP	Numerical Weather Prediction
TAMDE	Target Area Meteorological Data Experiment

Distribution

	Copies
Commandant U.S. Army Chemical School ATTN: ATZN-CM-CC (Mr. Barnes) Fort McClellan, AL 36205-5020	1
NASA Marshal Space Flight Center Deputy Director Space Science Laboratory Atmospheric Sciences Division ATTN: E501 (Dr. Fichtl) Huntsville, AL 35802	1
NASA/Marshall Space Flight Center Atmospheric Sciences Division ATTN: Code ED-41 Huntsville, AL 35812	1
Deputy Commander U.S. Army Strategic Defense Command ATTN: CSSD-SL-L (Dr. Lilly) P.O. Box 1500 Huntsville, AL 35807-3801	1
Deputy Commander U.S. Army Missile Command ATTN: AMSMI-RD-AC-AD (Dr. Peterson) Redstone Arsenal, AL 35898-5242	1
Commander U.S. Army Missile Command ATTN: AMSMI-RD-DE-SE (Mr. Lill, Jr.) Redstone Arsenal, AL 35898-5245	1

Commander
U.S. Army Missile Command
ATTN: AMSMI-RD-AS-SS (Mr. Anderson)   1
Redstone Arsenal, AL 35898-5253

Commander
U.S. Army Missile Command
ATTN: AMSMI-RD-AS-SS (Mr. B. Williams)   1
Redstone Arsenal, AL 35898-5253

Commander
U.S. Army Missile Command
Redstone Scientific Information Center
ATTN: AMSMI-RD-CS-R/Documents   1
Redstone Arsenal, AL 35898-5241

Commander
U.S. Army Aviation Center
ATTN: ATZQ-D-MA (Mr. Heath)   1
Fort Rucker, AL 36362

Commander
U.S. Army Intelligence Center
and Fort Huachuca
ATTN: ATSI-CDC-C (Mr. Colanto)   1
Fort Huachuca, AZ 85613-7000

Northrup Corporation
Electronics Systems Division
ATTN: Dr. Tooley   1
2301 West 120th Street, Box 5032
Hawthorne, CA 90251-5032

Commander
Pacific Missile Test Center
Geophysics Division
ATTN: Code 3250 (Mr. Battalino)   1
Point Mugu, CA 93042-5000

Commander
Code 3331
Naval Weapons Center
ATTN: Dr. Shlanta   1
China Lake, CA 93555

Lockheed Missiles & Space Co., Inc.
Kenneth R. Hardy
ORG/91-01 B/255   1
3251 Hanover Street
Palo Alto, CA 94304-1191

Commander
Naval Ocean Systems Center
ATTN: Code 54 (Dr. Richter)   1
San Diego, CA 92152-5000

Meteorologist in Charge
Kwajalein Missile Range
P.O. Box 67   1
APO San Francisco, CA 96555

U.S. Department of Commerce Center
Mountain Administration
Support Center, Library, R-51
Technical Reports
325 S. Broadway   1
Boulder, CO 80303

Dr. Hans J. Liebe
NTIA/ITS S 3
325 S. Broadway   1
Boulder, CO 80303

NCAR Library Serials
National Center for Atmos Research
P.O. Box 3000   1
Boulder, CO 80307-3000

Headquarters
Department of the Army
ATTN: DAMI-POI   1
Washington, DC 20310-1067

Mil Asst for Env Sci Ofc of
the Undersecretary of Defense
for Rsch & Engr/R&AT/E&LS
Pentagon - Room 3D129   1
Washington, DC 20301-3080

Headquarters
Department of the Army
DEAN-RMD/Dr. Gomez   1
Washington, DC 20314

Director
Division of Atmospheric Science
National Science Foundation
ATTN: Dr. Bierly   1
1800 G. Street, N.W.
Washington, DC 20550

Commander
Space & Naval Warfare System Command
ATTN: PMW-145-1G   1
Washington, DC 20362-5100

Director
Naval Research Laboratory
ATTN: Code 4110
(Mr. Ruhnke)   1
Washington, DC 20375-5000

Commandant
U.S. Army Infantry
ATTN: ATSH-CD-CS-OR (Dr. E. Dutoit)   1
Fort Benning, GA 30905-5090

USAFETAC/DNE   1
Scott AFB, IL 62225

Air Weather Service
Technical Library - FL4414   1
Scott AFB, IL 62225-5458

USAFETAC/DNE
ATTN: Mr. Glauber   1
Scott AFB, IL 62225-5008

Headquarters
AWS/DOO   1
Scott AFB, IL 62225-5008

Commander
U.S. Army Combined Arms Combat
ATTN: ATZL-CAW   1
Fort Leavenworth, KS 66027-5300

Commander
U.S. Army Space Institute
ATTN: ATZI-SI   1
Fort Leavenworth, KS 66027-5300

Commander
U.S. Army Space Institute
ATTN: ATZL-SI-D   1
Fort Leavenworth, KS 66027-7300

Commander
Phillips Lab
ATTN: PL/LYP (Mr. Chisholm)   1
Hanscom AFB, MA 01731-5000

Director
Atmospheric Sciences Division
Geophysics Directorate
Phillips Lab
ATTN: Dr. McClatchey   1
Hanscom AFB, MA 01731-5000

Raytheon Company
Dr. Sonnenschein
Equipment Division
528 Boston Post Road   1
Sudbury, MA 01776
Mail Stop 1K9

Director
U.S. Army Materiel Systems Analysis Activity
ATTN: AMXSY-CR (Mr. Marchetti)   1
Aberdeen Proving Ground, MD 21005-5071

Director
U.S. Army Materiel Systems Analysis Activity
ATTN: AMXSY-MP (Mr. Cohen)   1
Aberdeen Proving Ground, MD 21005-5071

Director
U.S. Army Materiel Systems Analysis Activity
ATTN: AMXSY-AT (Mr. Campbell)   1
Aberdeen Proving Ground, MD 21005-5071

Director
U.S. Army Materiel Systems
Analysis Activity
ATTN: AMXSY-CS (Mr. Bradley)   1
Aberdeen Proving Ground, MD 21005-5071

Director
ARL Chemical Biology
Nuclear Effects Division
ATTN: AMSRL-SL-CO   1
Aberdeen Proving Ground, MD 21010-5423

Army Research Laboratory
ATTN: AMSRL-D   1
2800 Powder Mill Road
Adelphi, MD 20783-1145

Army Research Laboratory
ATTN: AMSRL-OP-SD-TP   1
Technical Publishing
2800 Powder Mill Road
Adelphi, MD 20783-1145

Army Research Laboratory
ATTN: AMSRL-OP-CI-SD-TL   1
2800 Powder Mill Road
Adelphi, MD 20783-1145

Army Research laboratory
ATTN: AMSRL-SS-SH   1
(Dr. Sztankay)
2800 Powder Mill Road
Adelphi, MD 20783-1145

U.S. Army Space Technology
and Research Office
ATTN: Ms. Brathwaite   1
5321 Riggs Road
Gaithersburg, MD 20882

National Security Agency
ATTN: W21 (Dr. Longbothum)   1
9800 Savage Road
Fort George G. Meade, MD 20755-6000

OIC-NAVSWC
Technical Library (Code E-232)   1
Silver Springs, MD 20903-5000

Commander
U.S. Army Research office
ATTN: DRXRO-GS (Dr. Flood)   1
P.O. Box 12211
Research Triangle Park, NC 27009

Commander
U.S. Army Communications-Electronics
Center for EW/RSTA
ATTN: AMSEL-RD-EW-SP   1
Fort Monmouth, NJ 07703-5206

Commander
Department of the Air Force
OL/A 2d Weather Squadron (MAC)   1
Holloman AFB, NM 88330-5000

PL/WE   1
Kirtland AFB, NM 87118-6008

Director
U.S. Army TRADOC Analysis Center
ATTN: ATRC-WSS-R   1
White Sands Missile Range, NM 88002-5502

Director
U.S. Army White Sands Missile Range
Technical Library Branch
ATTN: STEWS-IM-IT   3
White Sands Missile Range, NM 88002

Army Research Laboratory
ATTN: AMSRL-BE (Mr. Veazy)   1
Battlefield Environment Directorate
White Sands Missile Range, NM 88002-5501

Army Research Laboratory
ATTN: AMSRL-BE-A (Mr. Rubio)   1
Battlefield Environment Directorate
White Sands Missile Range, NM 88002-5501

34

Army Research Laboratory
ATTN: AMSRL-BE-M (Dr. Niles)   1
Battlefield Environment Directorate
White Sands Missile Range, NM 88002-5501

Army Research Laboratory
ATTN: AMSRL-BE-W (Dr. Seagraves)   1
Battlefield Environment Directorate
White Sands Missile Range, NM 88002-5501

USAF Rome Laboratory Technical
Library, FL2810   1
Corridor W, STE 262, RL/SUL
26 Electronics Parkway, Bldg 106
Griffiss AFB, NY 13441-4514

AFMC/DOW   1
Wright-Patterson AFB, OH 03340-5000

Commandant
U.S. Army Field Artillery School
ATTN: ATSF-TSM-TA (Mr. Taylor)   1
Fort Sill, OK 73503-5600

Commander
U.S. Army Field Artillery School
ATTN: ATSF-F-FD (Mr. Gullion)   1
Fort Sill, OK 73503-5600

Commander
Naval Air Development Center
ATTN: Al Salik (Code 5012)   1
Warminister, PA 18974

Commander
U.S. Army Dugway Proving Ground
ATTN: STEDP-MT-M (Mr. Bowers)   1
Dugway, UT 84022-5000

Commander
U.S. Army Dugway Proving Ground
ATTN: STEDP-MT-DA-L   1
Dugway, UT 84022-5000

Defense Technical Information Center
ATTN: DTIC-OCP   2
Cameron Station
Alexandria, VA 22314-6145

Commander
U.S. Army OEC
ATTN: CSTE-EFS   1
Park Center IV
4501 Ford Ave
Alexandria, VA 22302-1458

Commanding Officer
U.S. Army Foreign Science & Technology Center
ATTN: CM   1
220 7th Street, NE
Charlottesville, VA 22901-5396

Naval Surface Weapons Center
Code G63   1
Dahlgren, VA 22448-5000

Commander and Director
U.S. Army Corps of Engineers
Engineer Topographics Laboratory
ATTN: ETL-GS-LB   1
Fort Belvoir, VA 22060

U.S. Army Topo Engineering Center
ATTN: CETEC-ZC   1
Fort Belvoir, VA 22060-5546

Commander
USATRADOC
ATTN: ATCD-FA   1
Fort Monroe, VA 23651-5170

TAC/DOWP   1
Langley AFB, VA 23665-5524

Commander
Logistics Center
ATTN: ATCL-CE   1
Fort Lee, VA 23801-6000

Science and Technology
101 Research Drive   1
Hampton, VA 23666-1340

Commander
U.S. Army Nuclear and Chemical Agency
ATTN: MONA-ZB, Bldg 2073   1
Springfield, VA 22150-3198

Record Copy   3

   Total   89